5
Corrosion resists Ni, Co co-pigmented nanoporous anodized alumina as spectral selective coating structure

5.1 Introduction

Anodized alumina with pigmented metals such as iron (Fe), cobalt (Co), nickel (Ni), copper (Cu), gold (Au), silver (Ag), molybdenum (Mo), chromium (Cr), and tungsten (W) are reported as SSACs with absorbance ≥0.90 and thermal emittance of 0.04 to 0.10 [Galione et al., 2010, Salmi et al., 2000, Wäckelgård, 1996, Andersson et al., 1980, Boström et al., 2003]. Ni-pigmented anodized alumina was reported as SSAC using the electrochemical deposition technique [Andersson et al., 1980; Kumar et al., 1983]. These SSACs exhibit thermal stability in 250 – 300 °C temperature range. Further, thermal stability can be enhanced by replacing Ni with cobalt as suggested by Cuevas et al. and Nahar et al. [Cuevas et al., 2014, Nahar et al., 1989]. Until now, Ni-Co co-pigmented bimetallic anodized alumina as SSAC has not been reported. In addition, studies on corrosion and thermal stability of these SSACs are not available in the literature. In this chapter, we will discuss the development of Ni, Co co-pigmented anodized alumina as a spectrally selective coating using the electrochemical deposition pathway, as well as its thermal stability and corrosion resistance. The microstructure, elementary composition, morphological and optical properties are also discussed in detail.

5.2 Experimental details

Ni and Co are co-pigmented in nanoporous anodized alumina by electroplating. The details of the deposition requirements are explained in subsection 3.2.3 of chapter 3. Electrodeposited sample of Ni, Co for 10 minutes in anodized alumina called sample B in this chapter. Sample B was subjected to heat treatment for 100 hours at 300 °C. For corrosion studies, the potentiodynamic spectrum was recorded in a solution containing 3.5% by weight of Sodium Chloride using Autolab electrochemical workstation (Metrohm make) where platinum and Ag / AgCl act as counter and reference electrodes.

Anodization is the formation of oxides on the surface of anode (metal) during the electrochemical reaction. Here, an oxide layer develops initially on the metal surface together with the nucleation of pores. The growth of the pores increases due to the locally generated heat because of high-electric field at these sites, together with heat generated due to the acid-catalyzed solution of the oxide [Li et al., 1998]. **Figure 5.1** shows the schematic diagram for the anodizing process. Faraday's electrolysis laws, given in equation (4.3) of chapter 4, are used to estimate the deposited mass of aluminum oxide. The calculated mass of Al_2O_3 ~ 0.0633 g, while the measured weight of deposit after anodization is approximately 0.0095g. The measured weight was lower than the calculated mass, suggesting a lower electrode performance. The efficiency of the electrode (ε_f) is defined by equation (4.6), chapter 4. Aluminum electrodes showed the yield of 14.33% ± 3.77%. Similarly, the theoretical deposited mass of Ni and Co is ~ 0.101 g, while the mass measured for the same is approximately 0.031 g after pigmentation. Again, the difference between the theoretical weight and the measured weight of Ni, and Co is attributed to lower electrode efficiency.

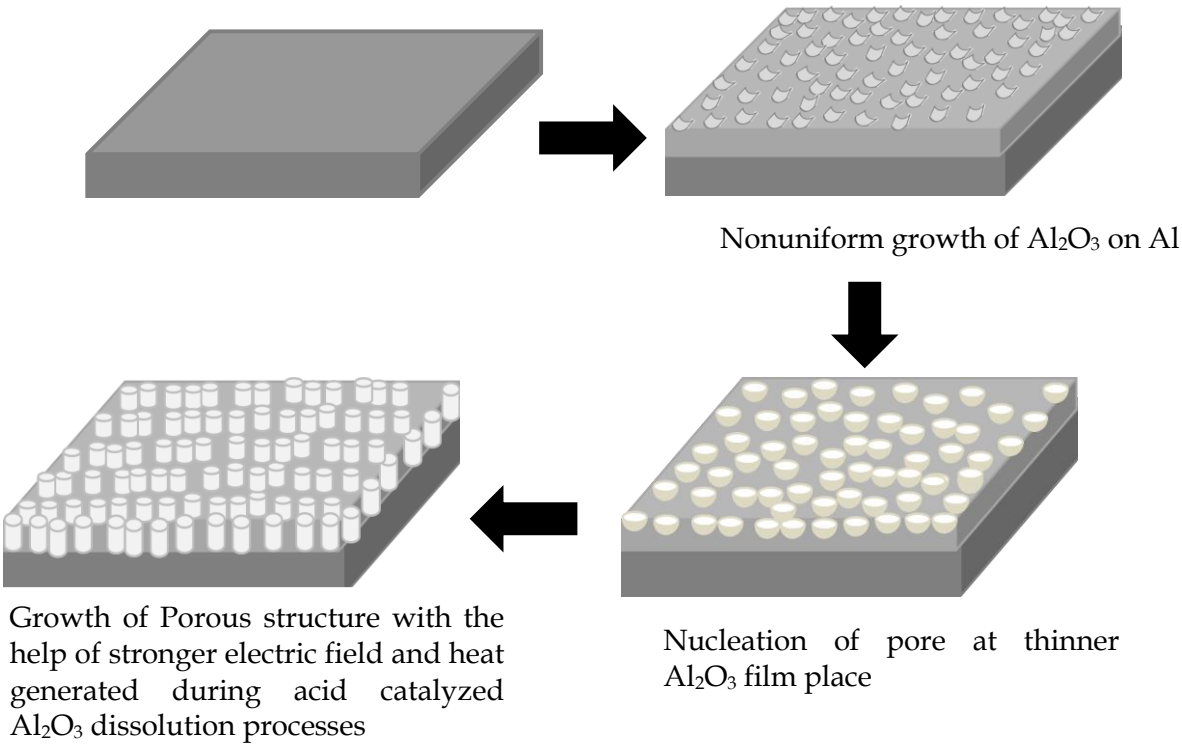

Figure 5.1 Schematic view of each step explaining the growth of nanoporous alumina structure on Al substrate

5.3 Optimization

A co-pigmentation process of Ni-Co was performed on an anodized alumina substrate for different time durations to optimize the optical properties. The NC-5m, NC-10m, and NC-15m samples represent an electrodeposited sample for Ni and Co co-pigmentation for 5, 10, and 15 minutes, respectively. Optical characterization was performed on co-pigmented samples, and the optical properties were compared to determine the optimized time for co-pigmentation**.** **Figure 5.2** shows the reflectance curve in the IR and UV-Vis range for these samples. The details of the optical properties recorded for these different samples are summarized in **Table 5.1**. The comparison of the optical properties of these selective solar coatings suggests that a sample with co-pigmentation for 10 m has an optimal absorptance. However, if the duration of pigmentation increases, it causes a slight decrease in absorptance, yet remains> 90%, but the emission deteriorates considerably from 0.14 to 0.17. Thus, 10-minute co-pigmentation showed the optimal optical properties i.e., for NC-10m sample.

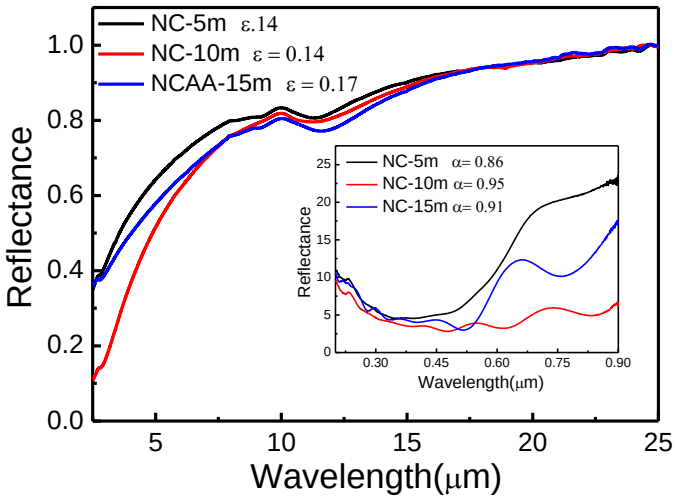

Figure 5.2 Reflectance with wavelength plot of samples deposited for different time duration

Table 5.1 Absorptance and emittance of samples deposited for different time duration

Sample	Absorptance (α)	Emittance (ε)
NC-5m	0.86	0.14
NC	0.95	0.14
NCAA-15m	0.91	0.17

5.4 Result and discussion

X-ray diffraction measurements (XRD) were performed to study the crystallographic structure of (i) anodized alumina (Sample A), (ii) Ni, Co co-pigmented anodized alumina optimized renamed as Sample B, (iii) heat treated (Sample C), and (iv) corrosion treated (Sample D) samples. **Figure 5.3** shows the respective XRD spectrum for these samples. The diffraction peaks for Al_2O_3 are observed at 2θ ~ 65.08° and 78.28°, correspond (220), and (311) planer orientations (ICDD number 04-0787). At 2θ ~ 38.4 ° and 44.84 °, the low diffraction peaks of Al_2O_3 correspond (111) and (200). These peaks of higher intensity were observed for corrosion and heat-treated samples. i.e sample C and D. This enhancement in the intensity of XRD peaks is attributed to the oxidation of the metallic part during heating and corrosion experiments. Also, no diffraction peaks are observed for Ni or Co metals, indicating the lower Ni and Co metal content in pigmented spectrally selective absorber structures.

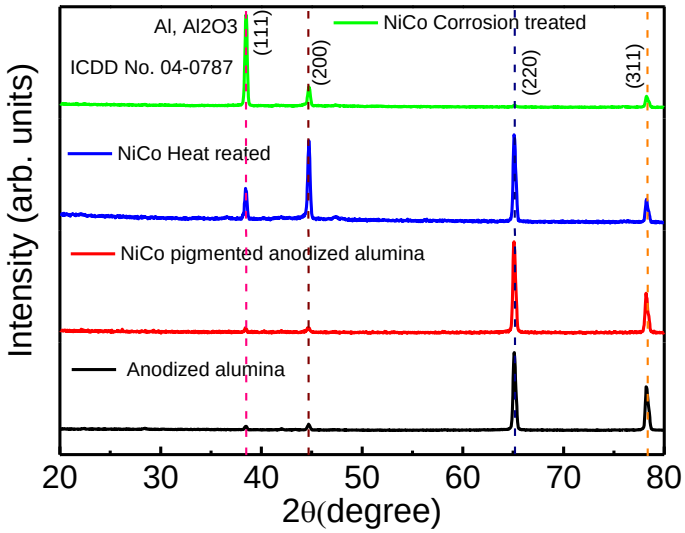

Figure 5.3 X-ray diffraction (XRD) plot of Sample A, Sample B, Sample C, and Sample D samples

Further, these co-pigmented SSACs are subjected to the surface-intensive microstructural and morphological measurements using SEM measurements. SEM measurements identify the nano-porous nature of alumina in all these Sample A, Sample B, Sample C, and Sample D samples (**Figure 5.4 (a, b, c & d)**). The estimated pore diameter using the FESEM measurement is shown in the box of **Figures 5.4(a & c),** and the pore diameters are approximately 45 ± 10 nm. The metals are electrochemically pigmented within the nanoporous anodized alumina (Sample A) structures. Pore openings are still visible even after Ni-Co co-pigmentation. A nanoporous structure can also be observed for heat-treated Sample C and corrosion treated Sample D. We also estimated the elemental composition for these coatings using EDX measurements. EDX measurements show the presence of metallic Ni and Co, as shown in the table in **Figure 5.4 (a, b, c & d)**. Inductively coupled plasma optical emission spectroscopy (ICP-OES) is used for elemental analysis of Sample B. The proportion of Co to Ni in the Sample B sample was found to be approximately 6.09. Detailed measurements of the ICP-OES experiment are given in **Table 5.2.** According to EDX and the ICP-OES measurements, NCAA sample had a larger fraction of

Co versus Ni. This higher fraction of Co after pigmentation could be attributed to the preferred electrodeposition of Co over Ni, although for electrochemical deposition, equimolar Co and Ni precursors are used.

Table 5.2 Measurement detail of ICP-OES experiment for Sample B

Sample ID	Element	wavelength	Concentration	Intensity	Uncorrected Concentration
Sample B	Ni	231.60	2.29	97599	2.29
	Co	228.61	14.00	559811	14.00

For surface morphological studies, AFM measurements are performed. Figure **5.5 (a, b, c & d)** shows 3D topographic images for Sample A, Sample B, Sample C, and Sample D, respectively. The surface roughness estimation is crucial as it affects the optical performance of the fabricated selective solar absorber. The observed RMS values of surface roughness are 108.4 nm, 31.27 nm, 57.24 nm, and 40.68 nm for Sample A, Sample B, Sample C, and Sample D, respectively, and indicated with respective AFM images. Lower surface roughness was observed for Sample B compared to anodized alumina Sample. It is due the metal pigmentation of nanoporous anodized alumina Sample A. However, an increase in surface roughness was observed for heat treated Sample C and corrosion treated Sample D. Oxidation of top layer in heat treated Sample C and corrosion treated sample D causes degradation i.e. enhancing the surface roughness. The AFM measurement analysis is suggesting the presence of nanoporous structures on fabricated spectrally selective solar absorber coating.

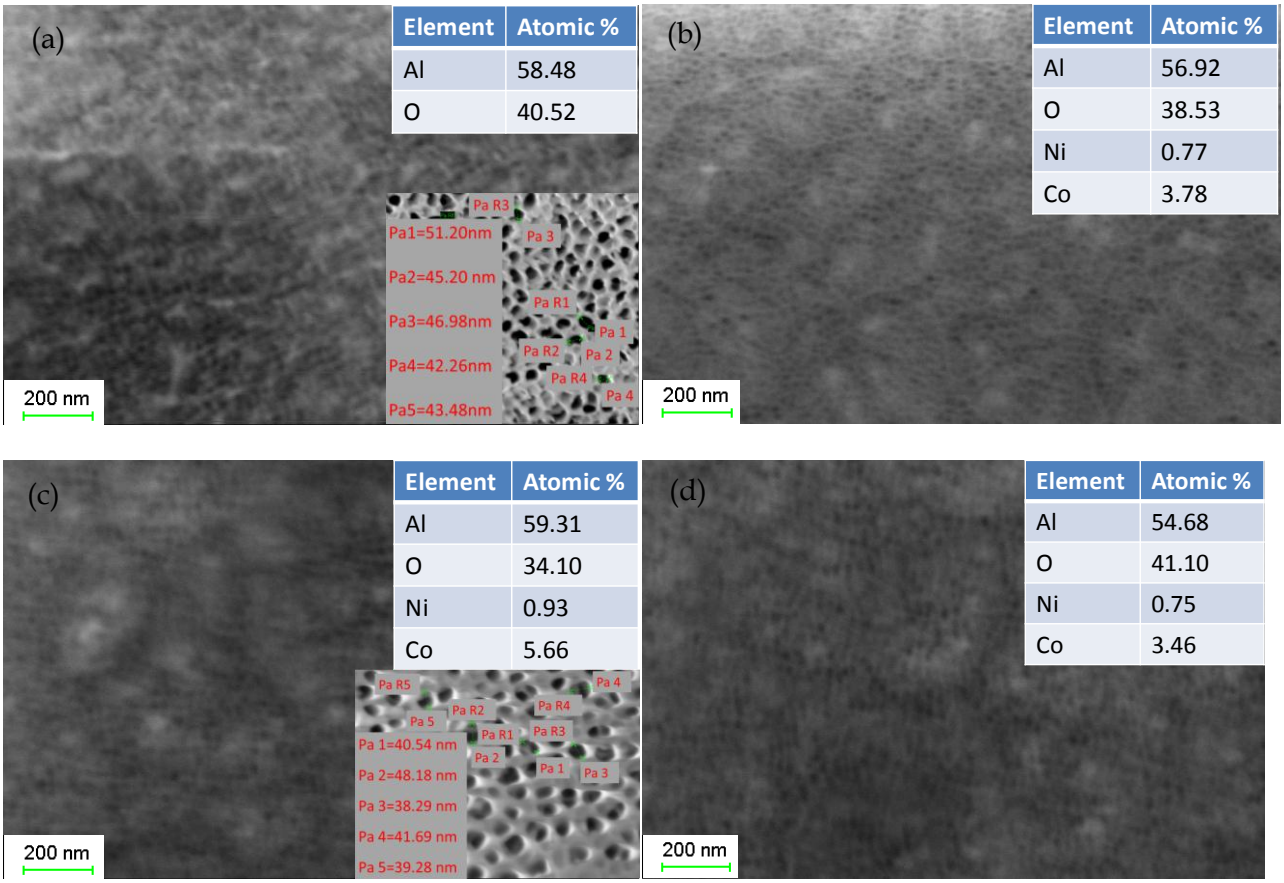

Figure 5.4 SEM images for (a) Sample A (b) Sample B (c) Sample C and (d) Sample D and elemental composition shown in inset. Inset FESEM image shows the nonoporous structure and its size

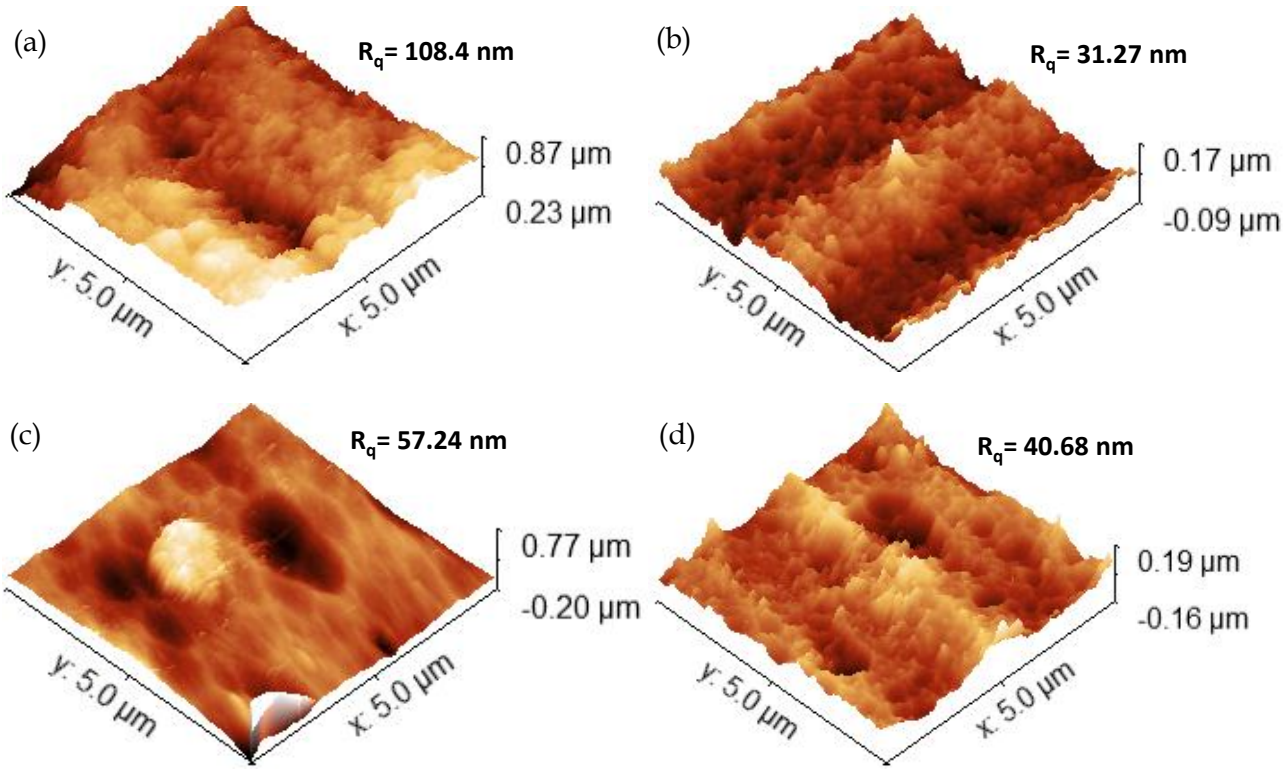

Figure 5.5 Three dimensional AFM topographic images of (a) Sample A (b) Sample B (c) Sample C and (d) Sample D with measured surface roughness

The vibrational spectrum of the fabricated SSAC structures is recorded using room temperature Raman measurements. **Figure 5.6 (a, b, c & d)** illustrates the vibrational spectrum of Sample A, Sample B, Sample C and Sample D. The peaks were located by curve fitting to identify the vibration mode present in the spectrum. **Figure 5.6(a)** shows the presence of strong peaks at approximately 335 cm^{-1} and several other weak peaks at 417 cm^{-1}, 468 cm^{-1}, 520 cm^{-1}, cm^{-1} and 719 cm^{-1}. These vibration modes correspond to the Al-O bonds in Al_2O_3 configured in tetrahedral structures [Thomas et al., 1989]. In the case of sample B pigmented with nickel, the presence of the vibration mode at 335, 510, 520 cm^{-1} corresponds to Al_2O_3 modes. The presence of Raman mode at ~ 550 cm^{-1} [Grinberga et al., 2007] corresponds to a Ni-O bond, suggesting the oxidation of the upper layer on which Ni is pigmented (**Figure 5.6 (b)**). **Figure 5.6 (c)** shows the vibrational spectrum for heat-treated Sample C, exhibiting new weak peaks at approximately 194, 483, 522, 620 $cm^{-1,}$ together with one strong peak at ~ 691 cm^{-1}. The weak peaks correspond to the Co-O bond, suggesting the presence of Co_3O_4 in sample C [Gwag & Sohn, 2012]. Cobalt oxidation is due to increased surface oxidation during the heat treatment. For corrosion treated i.e. Sample D, weak peaks were observed at 335, 509 cm^{-1}, and a relatively strong peak is noticed at 518 cm^{-1} (**Figure 5.6 (d)**). These Raman peaks correspond to Al_2O_3 vibration modes. The vibrational modes observed for these four samples are summarized in **Table 5.3**. After analyzing the Raman vibration peaks, we observed that the vibrational modes corresponding to the pigmentation of Ni and / or Co are present in the samples, as expected. Also, the presence of the Raman mode of Ni and Co oxide for heat and corrosion treated samples; suggests the partial oxidation of the metal content.

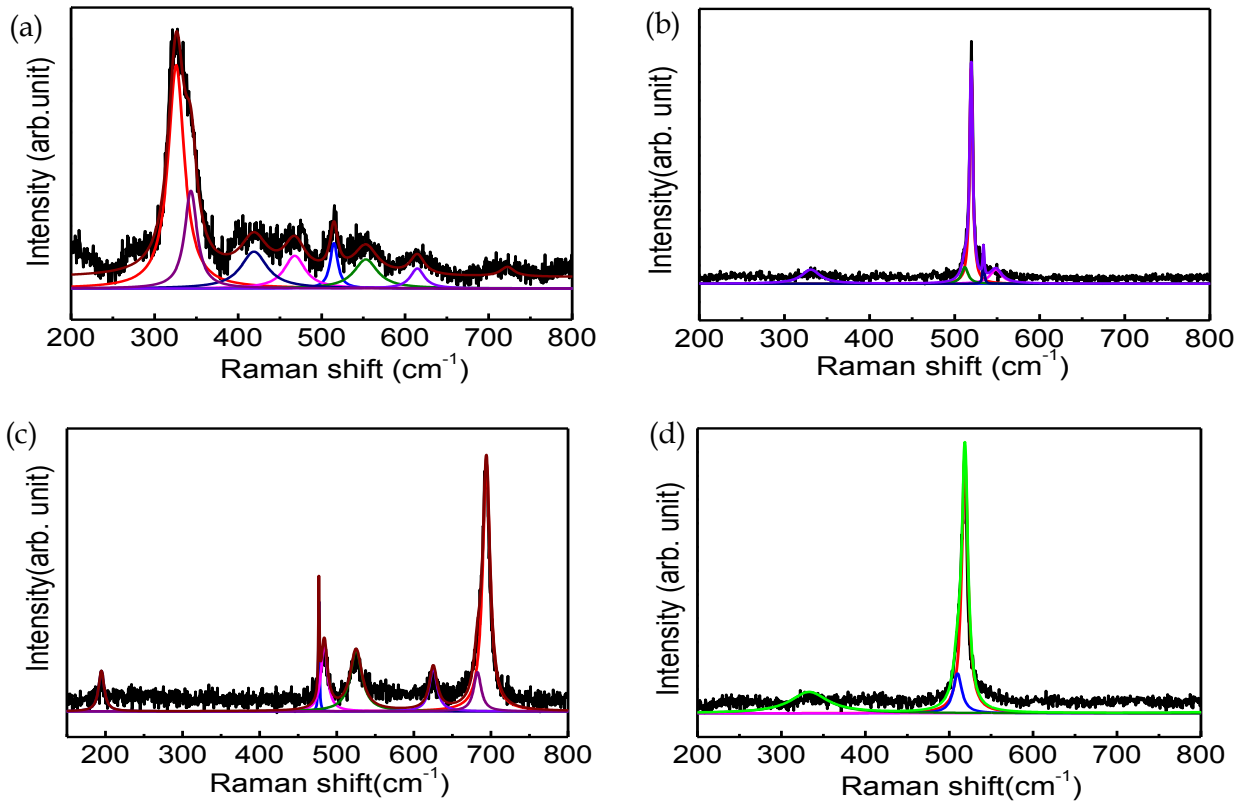

Figure 5.6 Raman spectrum of (a) Sample A (b) Sample B (c) Sample C and (d) Sample D at room temperature

Table 5.3 Detail of Raman measurement of Sample A, Sample B, Sample C and Sample D

Raman mode (cm-1)	Sample A	Sample B	Sample C	Sample D	Vibrational bond	Reference
194	X	X	√	X	Co-O	[Gwag & Sohn, 2012]
335	√	√	X	√	Al-O	[Thomas et al., 1989]
417	√	X	X	X	Al-O	
468	√	X	X	X	Al-O	
483	X	X	√	X	Co-O	[Gwag & Sohn, 2012)
509	X	√	X	√	Al-O	[Thomas et al., 1989]
520	√	√	√	√	Al-O	
550	√	X	X	X	Ni-O	[Grinberga et al., 2007]
619	√	X	√	X	Al-O	[Thomas et al., 1989]
682	X	X	√	X	Co-O	[Gwag & Sohn, 2012)
691	X	X	√	X	Co-O	[Gwag & Sohn, 2012)
719	√	X	X	X	Al-O	[Thomas et al., 1989]

The absorptance and emittance values for these Sample A, Sample B, Sample C, and Sample D were estimated using the reflectance measurement in the UV-Vis ranges (0.25 µm to 0.9 µm) and IR (2.5 to 25 µm). Equations (1.2) and (1.4) were followed for the calculation of absorption and emittance, respectively. **Figure 5.7** shows the FTIR spectra with the inset showing the respective UV-Vis spectra. The emittance is about 0.17 for Sample A, which after Ni-co co-pigmentation reduced to 0.14. The calculated absorptance for Sample B is ~ 0.95. **Table 5.4** summarizes the absorption and emittance for actors Sample A, Sample B, Sample C, and Sample D.

Table 5.4 Estimated absorptance and emittance of Sample A, Sample B, Sample C,and Sample D

Sample	Absorptivity (α)	Emissivity (ε)
Sample A	0.58	0.17
Sample B	0.95	0.14
Sample C	0.91	0.22
Sample D	0.89	0.38

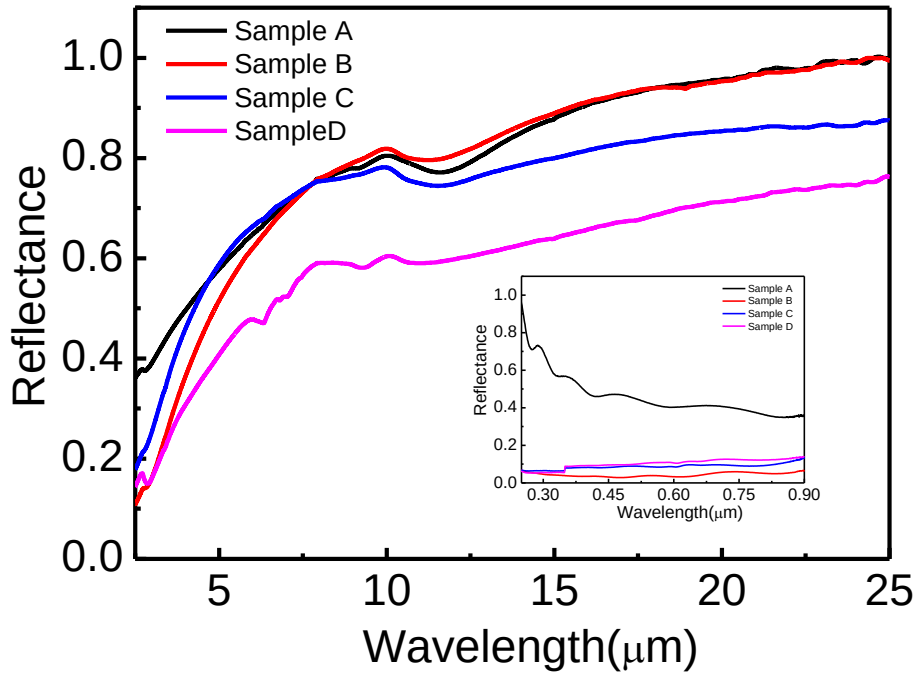

Figure 5.7 Reflectance plot against wavelength for Sample A, Sample B, Sample C, and Sample D in IR range together with inset showing reflectance in UV-Vis range

Further, the fabricated samples are heat-treated at 300 °C for 100 hours at atmospheric conditions to study the thermal stability. **Figure 5.8(a)** shows the schematic of heat treatment set up, and **Figure 5.8 (b)** shows the heat treatment profile used for the sample. UV-Vis and FTIR reflectance measurements were performed on heat-treated samples to estimate the absorptance and emittance (as shown in Figure 5.7). It was observed that the emittance for NCAA-HT sample increases from 0.14 to 0.22, whereas absorptance slightly reduced to 90% compared to 95% absorptance for NCAA sample. Also, the potentiodynamic measurement was performed for fabricated samples in saline water solution (containing 3.5 wt % NaCl) to understand the corrosion behavior. The enhancement in emittance similar to heat-treated sample was observed, however, absorptance remained nearly the same for the corrosion treated sample.

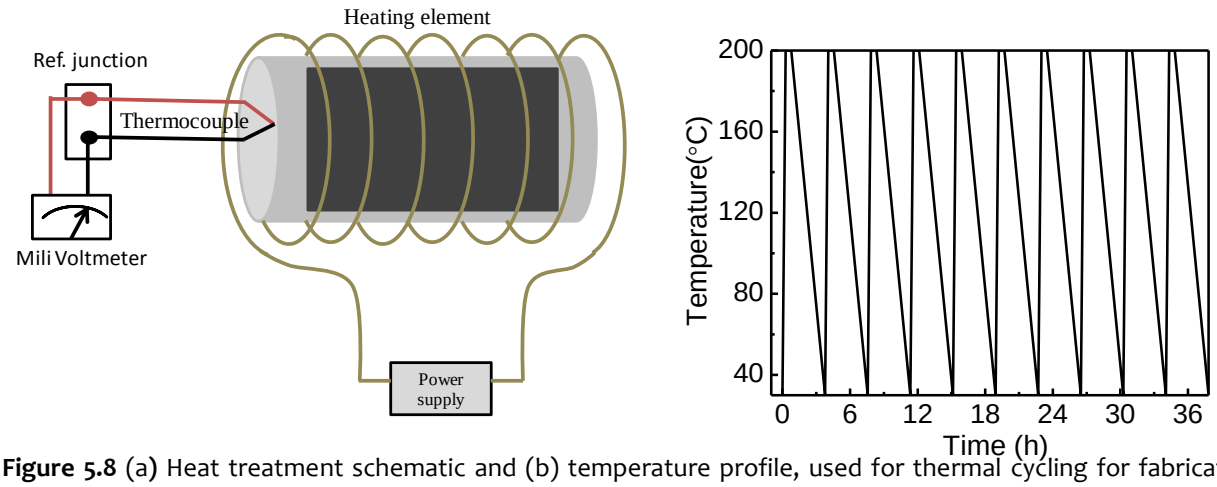

Figure 5.8 (a) Heat treatment schematic and (b) temperature profile, used for thermal cycling for fabricated Sample A

The detail of corrosion measurement is described in section 3.3.7 of chapter 3. All samples were immersed in a prepared electrolyte solution for 30 minutes duration for open circuit potential (OCP) establishment. The noted values of OCP for Sample A, Sample B, and Ni pigmented sample (named as Sample E) were -0.66, -0.69, and -0.71, respectively. The measurement scan was carried out in -1.5- 0 mV range to cover the OCP for all the samples. The potential versus current density plots are shown in **Figure 5.9** for Sample A, Sample B, and Sample E. The estimated corrosion parameters are summarized in **Table 5.5.** The polarization resistance calculated using Stern- Geary formula, equation 3.1. The shift in the breakdown potential of Sample A towards the positive side is observed with respect to Sample E sample. The observed passivation current density was the lowest for Sample A and the highest for Sample E (**Figure 5.9**). The calculated polarization resistance of Sample B was 5.33 kΩ, which is nearly twice as compared to that of polarization resistance for Sample E. The highest polarization resistance was observed for Sample A, which is almost nine times compared to NCAA sample. The lowest corrosion rate was observed for Sample A. Sample B shows lower corrosion resistance compared to Sample E (**Table 5.5**). The high corrosion resistance is shown by Sample B compared to Sample E may be due to the formation of Ni-Co alloy in the case of Ni, Co co-pigmented sample (Sample B). The absorptance for corrosion treated sample (Sample D) was nearly unaffected, whereas enhancement in emittance up to 0.38 was observed. The reflectance plots against wavelength are shown in **Figure 5.9(b)** and used to estimate the respective emittance values.

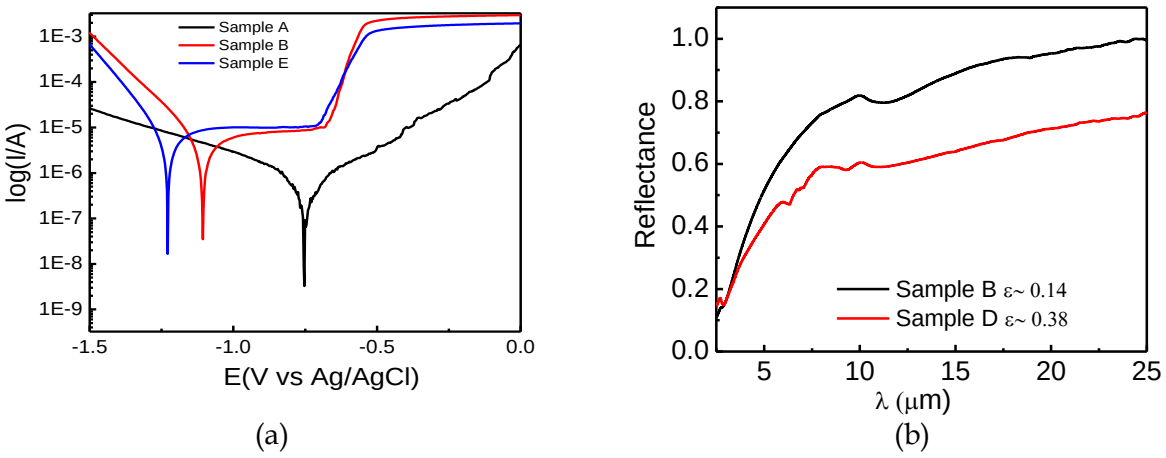

Figure 5.9 (a) Potential Vs current density plot for Sample A, Sample B and Sample E (b) reflectance plot with wavelength in IR range for sample B and Sample D

Table 5.5 Detail of measured corrosion parameter of Sample A, Sample B and Sample E

Sample	E_{corr} (V)	I_{corr} (μA/ cm^{-2})	R_p (kΩ)	C. Rate (mm/y)	b_a (mV/dec)	b_c (mV/dec)
Sample E	-1.22	2.74	2.41	0.029	99.36	158.17
Sample B	-1.10	2.17	5.33	0.023	106.19	209.31
Sample A	-0.75	0.27	45.61	0.008	148.12	171.19

Further, the corrosion behavior of fabricated Sample A, Sample B, and Sample E is corroborated by carrying out electrochemical impedance spectroscopy (EIS) analysis. The EIS measurements are performed at respective OCP of -0.72 mV, -0.82 mV and -0.83 mV for Sample A, Sample B, and Sample E, respectively over 0.1 Hz- 100 kHz frequency range using 10 mV ac source signal. **Figures 5.10(a & b)** show respective Nyquist and Bode plots for Sample A, Sample B, and Sample E. Figures **5.11(a, b & c)** show the best fitted equivalent circuit with impedance spectra for Sample A, Sample B, and Sample E, respectively. In the equivalent circuit, the double layer capacitance is represented by a constant phase element (CPE), solution, and polarization are represented by R_s and R_p, respectively. The corrosion resistance can be interpreted by polarization resistance. The diffusion in pores is represented by Warburg element (W). **Table 5.6** summarizes the computed values of CPE, R_s, R_p, and W for Sample A, Sample B, and Sample E. Here, the characterization of CPE is done using relation $1/Z_{CPE} = Y_{CPE} = Y_0.(j\omega)^N$, where Y_0 is the admittance and the exponent of CPE, related to frequency dispersion, is represented by N, which lies in 0 - 1 range. N = 1 indicates the pure capacitive and N= 0 resistive behavior. The highest polarization resistance was observed for Sample A compared to Sample B and Sample E. The presence of metallic particles may cause this behavior. High polarization resistance was also observed for Sample B compared to Sample E during the electrochemical corrosion experiment. Thus, EIS analysis also confirms the enhanced corrosive behavior for Sample B compared to Sample E.

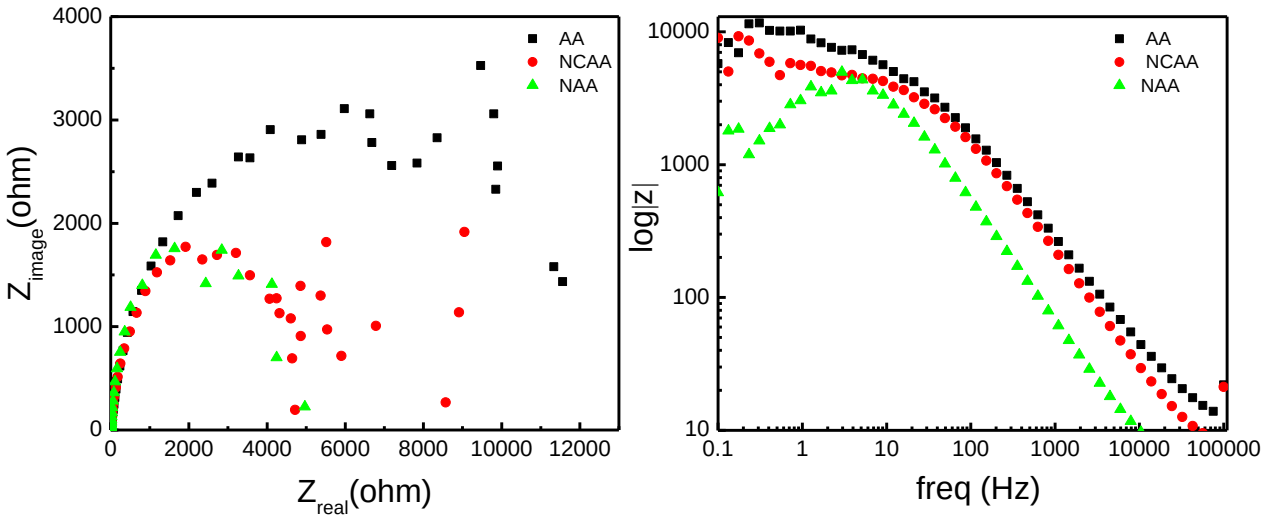

Figure 5.10 (a) Nyquist and (b) Bode plots of Sample A, Sample B and Sample E

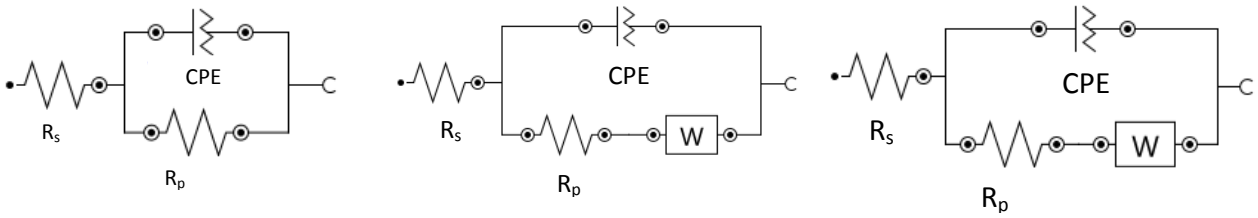

Figure 5.11 Equivalent circuit Sample A, Sample B, and Sample E

Table 5.6 Different Impedance parameters, estimated using equivalent circuit fitting of impedance data for Sample A, Sample B, and Sample E

Sample	R_s (ohm)	R_p (kohm)	CPE		W (mMho)
			Yo (µMho)	N	
Sample A	6.91	8.30	3.49	0.792	
Sample B	4.29	5.04	2.55	0.854	1.13
Sample E	4.10	1.51	4.44	0.926	1.10

5.5 Conclusion

The electrochemically developed Ni and Co co-pigmented anodized alumina structures showed high absorptance and low thermal emittance of ~ 0.95 and ~ 0.14, respectively. These structures showed high thermal stability up to 300°C in the open environment. The high corrosion resistance was observed compared to nickel anodized alumina structure. The absorptance after heat, as well as corrosion treatment, remained nearly the same, whereas emittance enhanced to ~ 0.2 and ~ 0.38, respectively. Thus, Ni-Co co-pigmented anodized alumina as spectrally selective coatings exhibit better thermal and corrosion stability compared to Ni pigmented structure in mid-temperature range up to 300 °C.